The Physics of Neutron Stars

J. M. Lattimer* and M. Prakash*

Neutron stars are some of the densest manifestations of massive objects in the universe. They are ideal astrophysical laboratories for testing theories of dense matter physics and provide connections among nuclear physics, particle physics, and astrophysics. Neutron stars may exhibit conditions and phenomena not observed elsewhere, such as hyperon-dominated matter, deconfined quark matter, superfluidity and superconductivity with critical temperatures near 10^{10} kelvin, opaqueness to neutrinos, and magnetic fields in excess of 10^{13} Gauss. Here, we describe the formation, structure, internal composition, and evolution of neutron stars. Observations that include studies of pulsars in binary systems, thermal emission from isolated neutron stars, glitches from pulsars, and quasi-periodic oscillations from accreting neutron stars provide information about neutron star masses, radii, temperatures, ages, and internal compositions.

The term "neutron star" as generally used today refers to a star with a mass M on the order of 1.5 solar masses ($M_\odot$), a radius R of ~12 km, and a central density n_c as high as 5 to 10 times the nuclear equilibrium density $n_0 \cong 0.16$ fm^{-3} of neutrons and protons found in laboratory nuclei. A neutron star is thus one of the densest forms of matter in the observable universe (*1*–*3*). Although neutrons dominate the nucleonic component of neutron stars, some protons (and enough electrons and muons to neutralize the matter) exist. At supranuclear densities, exotica such as strangeness-bearing baryons (*4, 5*), condensed mesons (pion or kaon) (*6*–*8*), or even deconfined quarks (*9*) may appear. Fermions, whether in the form of hadrons or deconfined quarks, are expected to also exhibit superfluidity and/or superconductivity.

Neutron stars encompass "normal" stars, with hadronic matter exteriors in which the surface pressure and baryon density vanish (the interior may contain any or a combination of exotic particles permitted by the physics of strong interactions), and "strange quark matter" (SQM) stars (*10*). An SQM star could have either a bare quark-matter surface with vanishing pressure but a large, supranuclear density, or a thin layer of normal matter supported by Coulomb forces above the quark surface. The name "SQM star" originates from the conjecture that quark matter with up, down, and strange quarks (the charm, bottom, and top quarks are too massive to appear inside neutron stars) might have a greater binding energy per baryon at zero pressure than iron nuclei have. If true, such matter is the ultimate ground state of matter. Normal matter is then metastable, and compressed to sufficiently high density, it would spontaneously convert to deconfined quark matter. Unlike normal stars, SQM stars are self-bound, not requiring gravity to hold them together. It is generally assumed that pulsars and other observed neutron stars are normal neutron stars. If SQM stars have a bare quark surface, calculations suggest that photon emission from SQM stars occurs primarily in the energy range 30 keV $< E <$ 500 keV (*11*).

How Neutron Stars are Formed

Neutron stars are created in the aftermath of the gravitational collapse of the core of a massive star (>8 $M_\odot$) at the end of its life, which triggers a Type II supernova explosion. Newly born neutron stars or proto–neutron stars are rich in leptons, mostly e^- and υ_e (Fig. 1). The detailed explosion mechanism of Type II supernovae is not understood (*12*), but it is probable that neutrinos play a crucial role. One of the most remarkable aspects is that neutrinos become temporarily trapped within the star during collapse. The typical neutrino-matter cross section is $\sigma \approx 10^{-40}$ cm^2, resulting in a mean free path $\lambda \approx (\sigma n)^{-1} \approx 10$ cm, where the baryon number density is $n \cong 2$ to 3 n_0. This length is much less than the proto–neutron star radius, which exceeds 20 km. The gravitational binding energy released in the collapse of the progenitor star's white dwarf–like core to a neutron star is about $3GM/5R^2 \cong 3 \times 10^{53}$ erg (G is the gravitational constant), which is about 10% of its total mass energy Mc^2. The kinetic energy of the expanding remnant is on the order of 1×10^{51} to 2×10^{51} erg, and the total energy radiated in photons is further reduced by a factor of 100. Nearly all the energy is carried off by neutrinos and antineutrinos of all flavors in roughly equal proportions.

Core collapse halts when the star's interior density reaches n_0, which triggers the formation of a shock wave at the core's outer edge. The shock wave propagates only about 100 to 200 km before it stalls, having lost energy to neutrinos and from nuclear dissociation of the material it has plowed through [stage (I) in Fig. 1]. Apparently, neutrinos from the core, assisted perhaps by rotation, convection, and magnetic fields, eventually resuscitate the shock, which within seconds accelerates outwards, expelling the massive stellar mantle. The proto–neutron star left behind rapidly shrinks because of pressure losses from neutrino emission in its periphery (stage II). The escape of neutrinos from the interior occurs on a diffusion time $\tau \cong 3R^2/\lambda c \approx 10$ s. The neutrinos observed from Supernova (SN) 1987A in the Large Magellanic Cloud confirmed this time scale and the overall energy release of $\cong 3 \times 10^{53}$ ergs (*13*–*16*).

The loss of neutrinos (which forces electrons and protons to combine, making the matter more neutron-rich) initially warms the stellar interior. The core temperature more than doubles (stage III), reaching ~50 MeV (6×10^{11} K). After 10 to 20 s, however, the steady emission of neutrinos begins to cool the interior. Because the cross section $\sigma \propto \lambda^{-1}$ scales as the square of the mean neutrino energy, the condition $\lambda > R$ is achieved in about 50 s. The star becomes transparent to neutrinos (stage IV), and its cooling rate accelerates.

Neutron stars have both minimum and maximum mass limits. The maximum mass, which is of purely general relativistic origin, is unknown, but lies in the range of 1.44 to 3 $M_\odot$. The upper bound follows from causality (*17*), that the speed of sound in dense matter is less than the speed of light, whereas the lower bound is the largest accurately measured pulsar mass, 1.4408 ± 0.0003 $M_\odot$, in the binary pulsar PSR 1913+16 (*18*). The minimum stable neutron star mass is about 0.1 $M_\odot$, although a more realistic minimum stems from a neutron star's origin in a supernova. Lepton-rich proto–neutron stars are unbound if their masses are less than about 1 $M_\odot$ (*19*).

The proto–neutron star, in some cases, might not survive its early evolution, collapsing instead into a black hole. This could occur in two different ways. First, proto–neutron stars accrete mass that has fallen through the shock. This accretion terminates when the shock lifts off, but not before the star's mass has exceeded its maximum mass. It would then collapse and its neutrino signal would

Department of Physics and Astronomy, State University of New York, Stony Brook, NY 11794–3800, USA.

*To whom correspondence should be addressed. E-mail: lattimer@mail.astro.sunysb.edu (J.M.L.); prakash@snare.physics.sunysb.edu (M.B.)

abruptly cease (*20*). If this does not occur, a second mode of black hole creation is possible (*21*). A proto–neutron star's maximum mass is enhanced relative to a cold star by its extra leptons and thermal energy. Therefore, following accretion, the proto–neutron star could have a mass below its maximum mass, but still greater than that of a cold star. If so, collapse to a black hole would occur on a diffusion time of 10 to 20 s, longer than in the first case. Perhaps such a scenario could explain the enigma of SN 1987A. The 10-s duration of the neutrino signal (*13*) confirmed the birth and early survival of a proto–neutron star, yet there is no evidence that a neutron star exists in this supernova's remnant. The remnant's observed luminosity is fully accounted for by radioactivity in the ejected matter (*22*), meaning that any contribution from magnetic dipole radiation, expected from a rotating magnetized neutron star, is very small. Either there is presently no neutron star, or its spin rate or magnetic field is substantially smaller than those of typical pulsars. A delayed collapse scenario could account for these observations (*21*).

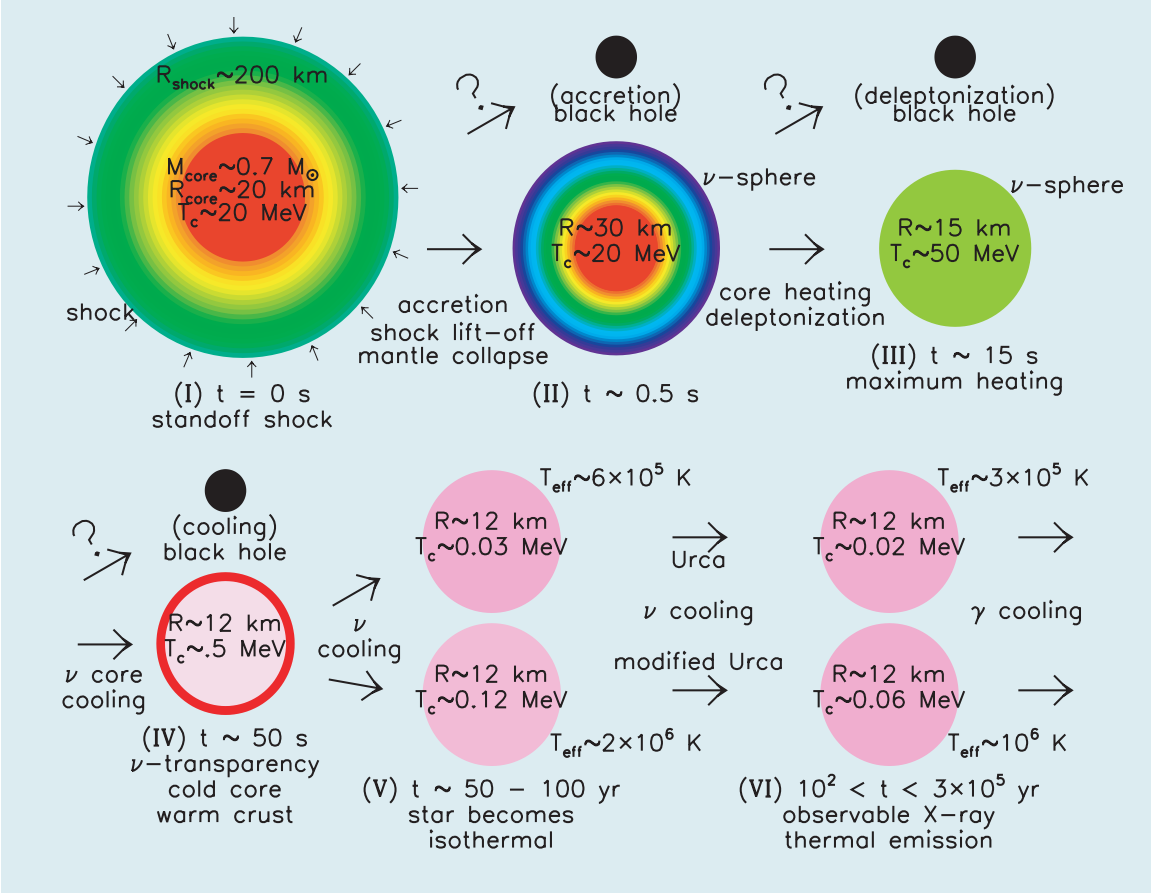

Fig. 1. The main stages of evolution of a neutron star. Roman numerals indicate various stages described in the text. The radius R and central temperatures T_c for the neutron star are indicated as it evolves in time t.

Global Structure of Neutron Stars

Global aspects of neutron stars, such as the mass-radius (M-R) relation, are determined by the equations of hydrostatic equilibrium. For a spherical object in general relativity (GR), these are the so-called TOV (Tolman-Oppenheimer-Volkov) equations (*23*, *24*):

$$\frac{dP}{dr} = -\frac{G(m(r) + 4\pi r^3 P/c^2)(\rho + P/c^2)}{r(r - 2Gm(r)/c^2)}, \qquad \frac{dm(r)}{dr} = 4\pi\rho r^2 \tag{1}$$

where P and ρ are the pressure and mass-energy density, respectively, and $m(r)$ is the gravitational mass enclosed within a radius r. Although a few exact solutions are known (*25*), for a realistic P-ρ relation (equation of state, EOS) these equations must be numerically solved to obtain the $M-R$ relation, as shown in Fig. 2. The region in Fig. 2 bounded by the Schwarzschild condition $R \leq 2GM/c^2$ is excluded by general relativity, and that bounded by $R \lesssim 3GM/c^2$ is excluded by causality (*26*). Some normal neutron star cases, such as GS1, contain large amounts of exotica, any of which produces a large amount of softening and relatively small radii and maximum masses. For small masses, SQM stars are nearly incompressible ($R \propto M^{1/3}$).

For normal neutron stars, the radius is relatively insensitive to the mass in the vicinity of 1 to 1.5 $M_\odot$ unless the maximum mass is relatively small. A simultaneous measurement of mass and radius of an intermediate-mass star could help to discriminate among the families of possible EOSs. Perhaps two of the most important, but unknown, astrophysical quantities are the neutron star maximum mass and the radius of 1.4 $M_\odot$ neutron stars.

There are large variations in predicted radii and maximum masses (Fig. 2) because of the uncertainties in the EOS near and above n_0 (*27*). This seems paradoxical because the properties of matter inside laboratory nuclei are thought to be well understood. However, an important distinction between nuclear and neutron star matter is their relative proton fraction x. Nuclear matter has nearly equal numbers of neutrons and protons ($x \cong 1/2$), but neutron star matter has only a few percent protons. The energy can be described with a quadratic interpolation in the proton fraction x:

$$E(n,x) = E(n,x = 1/2) + S_v(n)(1 - 2x)^2 \tag{2}$$

The symmetry energy function $S_v(n)$ is uncertain, although weak constraints exist from ground-state masses (binding energies) and giant dipole resonances of laboratory nuclei. The symmetry energy of nuclei is divided between bulk and surface contributions, which scale with nuclear mass number as A and $A^{2/3}$, respectively, but the ranges of $A^{1/3}$ (up to 6) and x in laboratory nuclei are too small to separate them.

A consequence of this uncertainty is that different models predict up to a factor of 6 variation in the pressure of neutron star matter near n_0, even though the pressure of symmetric matter is better known, being nearly zero at the same density.

This pressure variation accounts for the nearly 50% variation in predictions of neutron star radii (*27*).

A potential constraint on the EOS derives from the rotation of neutron stars. An absolute upper limit to the neutron star spin frequency is the mass-shedding limit, at which the velocity of the stellar surface equals that of an orbiting particle suspended just above the surface. For a rigid Newtonian sphere, this frequency is the Keplerian rate

$$\nu_K = (2\pi)^{-1}\sqrt{GM/R^3} = 1833(M/M_\odot)^{1/2}(10\ \mathrm{km}/R)^{3/2}\ \mathrm{Hz} \quad (3)$$

However, both deformation and GR effects are important. A similar expression, but with a coefficient of 1224 Hz and in which M and R refer to the mass and radius of the maximum-mass, nonrotating configuration, describes the maximum rotation rate possible for an EOS (*26*, *28*, *29*). We have found that Eq. 3, but with a coefficient of 1045 Hz, approximately describes the maximum rotation rate for a star of mass M (not close to the maximum mass) and nonrotating radius R independently of the EOS. The highest observed spin rate, 641 Hz from pulsar PSR B1937+21 (*30*), implies a radius limit of 15.5 km for 1.4 $M_\odot$.

Internal Structure and Composition

A neutron star has five major regions: the inner and outer cores, the crust, the envelope, and the atmosphere (Fig. 3). The atmosphere and envelope contain a negligible amount of mass, but the atmosphere plays an important role in shaping the emergent photon spectrum, and the envelope crucially influences the transport and release of thermal energy from the star's surface. The crust, extending about 1 to 2 km below the surface, primarily contains nuclei. The dominant nuclei in the crust vary with density, and range from ^{56}Fe for matter with densities less than about 10^6 g cm^{-3} to nuclei with $A \sim 200$ but $x \sim$ (0.1 to 0.2) near the core-crust interface at $n \approx n_0/3$. Such extremely neutron-rich nuclei are not observed in the laboratory, but rare-isotope accelerators (*31*) hope to create some of them.

Within the crust, at densities above the neutron drip density 4×10^{11} g cm^{-3} where the neutron chemical potential (the energy required to remove a neutron from the filled sea of degenerate fermions) is zero, neutrons leak out of nuclei. At the highest densities in the crust, more of the matter resides in the neutron fluid than in nuclei. At the core-crust interface, nuclei are so closely packed that they are almost touching. At somewhat lower densities, the nuclear lattice can turn inside-out and form a lattice of voids, which is eventually squeezed out at densities near n_0 (*32*). If so, beginning at about 0.1 n_0, there could be a continuous change of the dimensionality of matter from three-dimensional (3D) nuclei (meatballs), to 2D cylindrical nuclei (spaghetti), to 1D slabs of nuclei interlaid with planar voids (lasagna), to 2D cylindrical voids (ziti), to 3D voids (ravioli, or Swiss cheese in Fig. 3) before an eventual transition to uniform nucleonic matter (sauce). This series of transitions is known as the nuclear pasta.

For temperatures less than ~0.1 MeV, the neutron fluid in the crust probably forms a $^1S_0$ superfluid (*1*, *2*). Such a superfluid would alter the specific heat and the neutrino emissivities of the crust, thereby affecting how neutron stars cool. The superfluid would also form a reservoir of angular momentum that, being loosely coupled to the crust, could cause pulsar glitch phenomena (*33*).

The core constitutes up to 99% of the mass of the star (Fig. 3). The outer core consists of a soup of nucleons, electrons, and muons. The neutrons could form a $^3P_2$ superfluid and the protons a $^1S_0$ superconductor within the outer core. In the inner core, exotic particles such as strangeness-bearing hyperons and/or Bose condensates (pions or kaons) may become abundant. It is possible that a transition to a mixed phase of hadronic and deconfined quark matter develops (*34*), even if strange quark matter is not the ultimate ground state of matter. Delineating the phase structure of dense cold quark matter (*35*) has yielded novel states of matter, including color-superconducting phases with (*36*) and without condensed mesons (*35*).

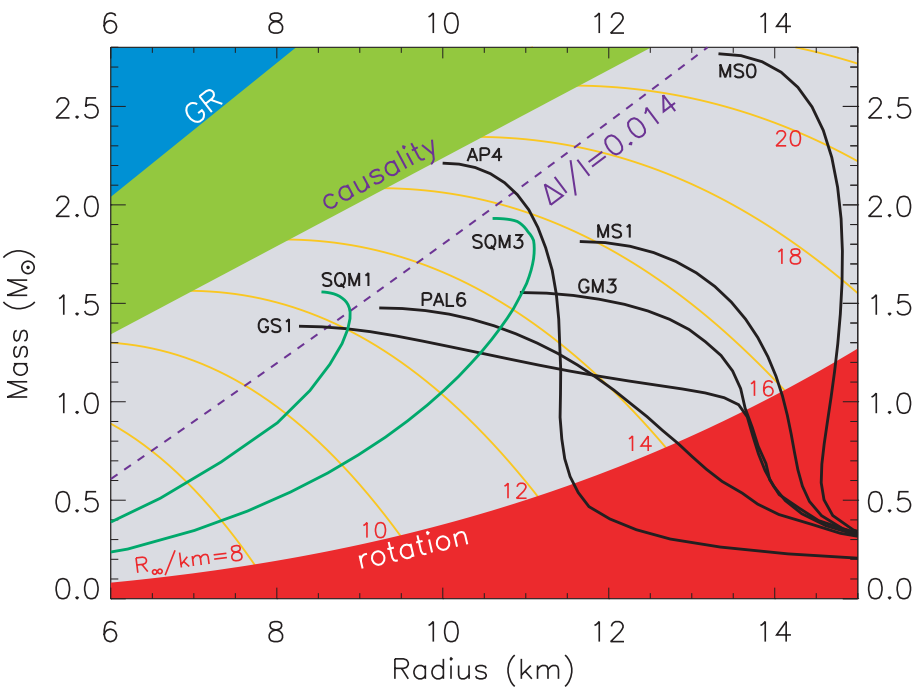

Fig. 2. Mass-radius diagram for neutron stars. Black (green) curves are for normal matter (SQM) equations of state [for definitions of the labels, see (*27*)]. Regions excluded by general relativity (GR), causality, and rotation constraints are indicated. Contours of radiation radii R_∞ are given by the orange curves. The dashed line labeled $\Delta I/I = 0.014$ is a radius limit estimated from Vela pulsar glitches (*27*).

Neutron Star Cooling

The interior of a proto–neutron star loses energy at a rapid rate by neutrino emission. Within 10 to 100 years, the thermal evolution time of the crust, heat transported by electron conduction into the interior, where it is radiated away by neutrinos, creates an isothermal structure [stage (V) in Fig. 1]. The star continuously emits photons, dominantly in x-rays, with an effective temperature T_{eff} that tracks the interior temperature but that is smaller by a factor of ~100. The energy loss from photons is swamped by neutrino emission from the interior until the star becomes about 3×10^5 years old (stage VI).

The overall time that a neutron star will remain visible to terrestrial observers is not yet known, but there are two possibilities: the standard and enhanced cooling scenarios. The dominant neutrino cooling reactions are of a general type, known as Urca processes (*37*), in which thermally excited particles alternately undergo beta and inverse-beta decays. Each reaction produces a neutrino or antineutrino, and thermal energy is thus continuously lost.

The most efficient Urca process is the direct Urca process involving nucleons:

$$n \rightarrow p + e^- + \bar{\nu}_e, \quad p \rightarrow n + e^+ + \nu_e \quad (4)$$

This process is only permitted if energy and momentum can be simultaneously conserved. This requires that the proton-to-neutron ratio exceeds 1/8, or the proton fraction $x \geq 1/9$, which is far above the value found in neutron star matter in the vicinity of n_0. In a mixture of neutrons, protons and electrons, the proton fraction x in beta equilibrium satisfies (*38*)

$$x \cong 0.048[S_v(n)/S_v(n_0)]^3(n_0/n)(1-2x)^3 \quad (5)$$

where, typically, $S_v(n_0) \cong 30$ MeV. Because x generally increases with density, the direct Urca process might still occur above some density threshold. However, if the direct process is not possible, neutrino cooling must occur by the modified Urca process

$$n + (n, p) \rightarrow p + (n, p) + e^- + \bar{\nu}_e.$$
$$p + (n, p) \rightarrow n + (n, p) + e^+ + \nu_e \quad (6)$$

in which an additional nucleon (n,p) participates in order to conserve momentum. The modified Urca rate is reduced by a factor of $(T/\mu_n)^2 \lesssim 10^{-4}$ to 10^{-5} compared to the direct Urca rate, and neutron star cooling is correspondingly slower. The standard cooling scenario assumes that direct Urca processes cannot occur and predicts that neutron stars should remain observable by surface thermal emission for up to a few million years.

The question of whether or not the direct Urca process occurs in neutron stars is of fundamental importance. The density dependence of the symmetry energy function S_v determines the values of x and the threshold density at which the nucleonic direct Urca process occurs (Eq. 5). It also plays an essential role in determining the threshold densities of other particles, such as hyperons, pions, kaons, or quarks, whose existences trigger other direct Urca processes (*37*). If a star's central density lies below the Urca threshold, enhanced cooling cannot occur. Again, the quantity $S_v(n)$ plays a crucial role for neutron stars, and its inherent uncertainty means that it is presently unknown if direct Urca processes can occur in neutron stars.

There are two additional issues affecting cooling trajectories of neutron stars: superfluidity (*39*, *40*) and envelope composition (*41*). Superfluidity quenches cooling from the direct Urca process. However, an additional cooling source from the formation and breaking of nucleonic Cooper pairs increases the cooling rate from the modified Urca process (*42*). Nevertheless, a clear distinction remains between enhanced and standard cooling trajectories.

Envelope composition also plays a role in the inferred surface temperatures. Although it is commonly assumed that the envelope is dominated by iron-peak nuclei, this may not be the case. Light elements (H or He) have smaller photon opacities, which enhance surface photon emission. Neutron stars appear warmer with light-element envelopes for their first 100,000 years of cooling, but eventually the situation reverses (*43*).

Observations and Inferred Stellar Properties

Masses. The most accurately measured neutron star masses are from timing observations of radio binary pulsars (*44*). These include pulsars orbiting another neutron star, a white dwarf, or a main-sequence star. Ordinarily, observations of pulsars in binaries yield orbital sizes and periods from Doppler shift phenomenon, from which the total mass of the binary can be deduced. But the compact nature of several binary pulsars permits detection of relativistic effects, such as Shapiro delay (*45*) or orbit shrinkage due to gravitational radiation reaction, which constrains the inclination angle and permits measurement of each mass in the binary. A sufficiently well-observed system, such as the binary pulsar PSR 1913+16 (*18*) or the newly discovered double pulsar binary PSR J0737-3039 (*46*), can have masses determined to impressive accuracy. Masses can also be estimated for neutron stars that are accreting matter from a stellar companion in so-called x-ray binaries, but the measurements have much larger relative errors (Table 1). Neutron stars in binaries with white dwarf companions have a broader range of masses than binary neutron stars, and the wider mass range may signify a wider range of formation mechanisms. It has been suggested that a rather narrow set of evolutionary circumstances conspire to form double neutron star binaries (*47*). The largest apparent masses are in the systems 4U1700-37, which might in fact contain a black hole, not a neutron star, Vela X-1, and the pulsar J0751+1807, but all have large uncertainties. Raising the limit for the neutron star maximum mass could eliminate entire EOS families, especially those in which exotica appear and substantial softening begins around 2 to 3 n_0. This could be significant, because exotica generally reduce the maximum mass appreciably.

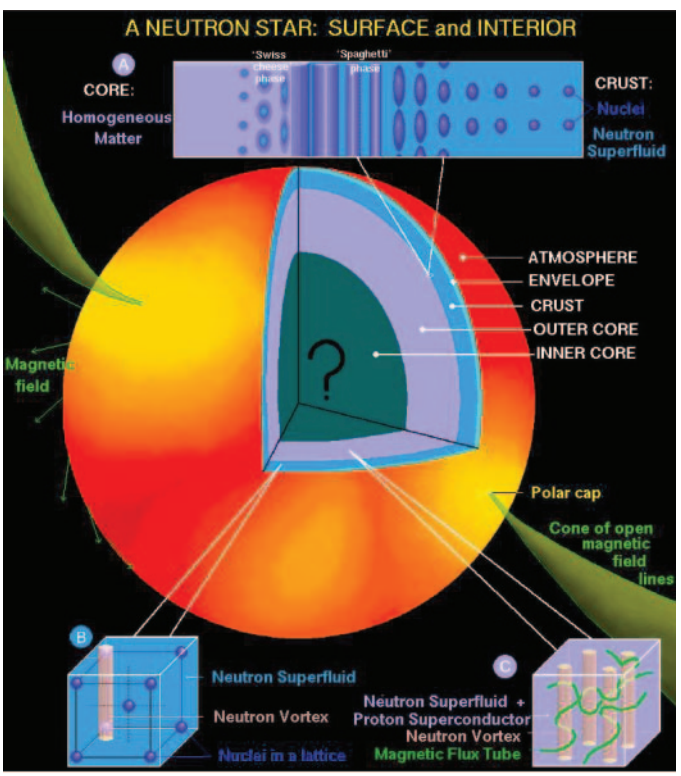

Fig. 3. The major regions and possible composition inside a normal-matter neutron star. The top bar illustrates expected geometric transitions from homogeneous matter at high densities in the core to nuclei at low densities in the crust. Superfluid aspects of the crust and outer core are shown in the insets. [Figure courtesy D. Page]

Thermal emission. Most known neutron stars are observed as pulsars and have photon emissions from radio to x-ray wavelengths dominated by nonthermal emissions. It is believed that the bulk of the nonthermal emissions are generated in a neutron star's magnetosphere. Although such emissions can teach us about magnetospheric phenomena, they are difficult to utilize in constraining the star's global aspects, such as mass, radius, and temperature, that have a significant bearing on a star's interior structure, composition, and evolution. About a dozen neutron stars with high thermal emissions, and with ages up to a million years, have been identified (*43*), and these stars are expected in the standard cooling scenario to have surface temperatures in the range of 3×10^5 to 10^6 K (Fig. 4), so the bulk of their emitted radiation should lie in the extreme ultraviolet or x-ray regions.

The effective temperature $T_{\mathrm{eff},\infty}$ is defined from

$$F_\infty = L_\infty/4\pi d^2 = \sigma_B T_{\mathrm{eff},\infty}^4 (R_\infty/d)^2 \quad (7)$$

where σ_B is the Stefan-Boltzmann constant, d is the distance, and F_∞ and L_∞ refer to the flux and luminosity observed at Earth. These lat-

ter quantities, and $T_{\mathrm{eff},\infty}$, are redshifted from the neutron star surface, where the redshift is $z = (1 - 2GM/Rc^2)^{-1} - 1$. For example, $T_{\mathrm{eff},\infty} = T_{\mathrm{eff}}/(1 + z)$ and $F_\infty = F/(1 + z)^2$. As a result, the so-called radiation radius R_∞, a quantity that can be estimated if F_∞, $T_{\mathrm{eff},\infty}$, and d are known, is defined to be $R_\infty = R(1 + z)$. R_∞ is a function of the mass and radius of the neutron star, but if redshift information is available, perhaps from spectral lines, M and R could be separately determined. Indeed, observation of spectral lines has been reported from 1E 1207.4-5209 (*48*) and EXO 0748-676 (*49*), but the identifications of the lines are controversial (*50*), with redshifts ranging from 0.12 to 0.35.

A serious hurdle in the attempt to determine R_∞ and $T_{\mathrm{eff},\infty}$ is the fact that neutron stars are not blackbodies (*51*, *52*). The star's atmosphere rearranges the spectral distribution of emitted radiation. Although models of neutron star atmospheres for a variety of compositions have been constructed, these are mostly limited to nonmagnetized atmospheres. Pulsars, however, are thought to have magnetic field strengths on the order of 10^{12} G or greater (*44*). The behavior of strongly magnetized hydrogen is relatively simple, but models of magnetized heavy-element atmospheres are still in a state of infancy (*53*).

A useful constraint on models is provided by a few cases in which the neutron star is sufficiently close to Earth for optical thermal emission to be detected (distinguished by green boxes in Fig. 4). These stars have optical fluxes several times less than what a blackbody extrapolation from the observed x-rays into the Rayleigh-Jeans optical domain would imply. This optical deficit is a natural consequence of the neutron star atmosphere and results in an inferred R_∞ greater than that deduced from a blackbody. In most cases, a heavy-element atmosphere adequately fits the global spectral distributions from x-ray to optical energies while also yielding neutron star radii in a plausible range. However, the observed absence of narrow spectral features, predicted by heavy-element atmosphere models, is puzzling (*54*, *55*). The explanation could lie with broadening or elimination of spectral features caused by intense magnetic fields or high pressures.

Radius estimates from isolated neutron stars, while falling into a plausible range, are also hampered by distance uncertainties. Pulsar distances can be estimated by dispersion measures (*44*), but these have uncertainties of 50% or more. In a few cases, such as Geminga (*56*), RX J185635-3754 (*57*, *58*) and PSR B0656+14 (*59*), parallax distances have been obtained, but errors are still large.

The recent discovery of thermal radiation from quiescent x-ray bursters (involving neutron stars in binaries) in globular clusters is particularly exciting. At first glance, it seems strange that neutron stars in globular clusters, which are on the order of 10 billion years old, could be hot enough to emit observable thermal radiation. However, it is believed that recent episodes of mass accretion from their companions have been a literal fountain of youth, replenishing their reservoir of thermal energy (*60*). The measurements of radii from these stars might become relatively precise, especially if the distances to the globular clusters in which they are found can be refined. Values of R_∞ in the range of 13 to 16 km have been estimated from the quiescent x-ray sources in the globular clusters NGC 5139 and 47 Tuc (*61*, *62*).

Theoretical cooling curves can be compared to observations if ages for the thermally emitting neutron stars can be estimated (Fig. 4). The best-determined ages are those for which dynamical information, such as observed space velocities coupled with a known birthplace, is available. Characteristic spin-down ages estimated from pulsar periods P and spin-down rates $\dot{P}$ using $\tau_s = P/2\dot{P}$ (*44*) are less reliable. In the cases in which both kinds of age estimates are available, they are generally discrepant by factors of 2 to 3.

Theoretical cooling tracks, for a variety of mass, radius, and superfluid properties, are relatively narrowly confined as long as enhanced cooling does not occur (*43*). These tracks are mostly sensitive to envelope composition. When enhanced cooling is considered, cooling tracks fall in a much wider range (Fig. 4). Although most observed stars are consistent with the standard cooling scenario, a few cases, espcially PSR J0205+6449 in 3C58 for which only upper limits to temperature and luminosity exist (*63*), may suggest enhanced cooling. Uncertainties in estimated temperature and ages have precluded definitive restrictions on EOSs or superfluid properties from being made.

Glitches. Pulsars provide several sources of information concerning neutron star properties. The fastest spinning pulsars yield constraints on neutron star radii. Ages and magnetic field strengths can be estimated from P and $\dot{P}$ measurements. Another rich source of data are pulsar glitches, the occasional disruption of the otherwise regular pulses (*44*). Although the origin of glitches is unknown, their magnitudes and stochastic behavior suggest they are global phenomena (*64*). The leading glitch model involves angular momentum transfer in the crust from the superfluid to the normal component (*33*). Both are spinning, but the normal crust is decelerated by the pulsar's magnetic dipole radiation. The superfluid is weakly coupled with the normal matter, and its rotation rate is not diminished. But when the difference in spin rates becomes too large, something breaks and the spin rates are brought into closer

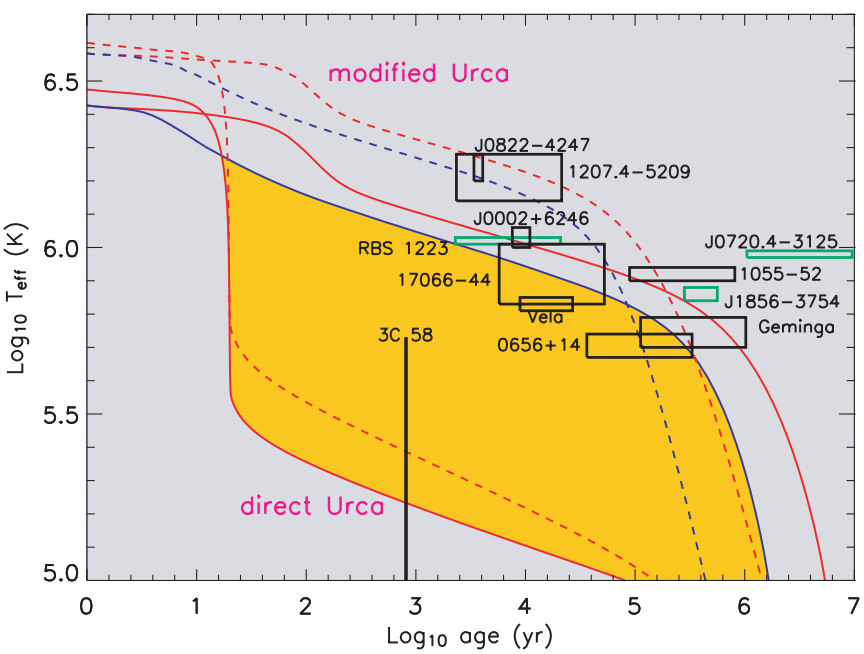

Fig. 4. Observational estimates of neutron star temperatures and ages together with theoretical cooling simulations for $M = 1.4\ M_\odot$. Models (solid and dashed curves) and data with uncertainties (boxes) are described in (*43*). The green error boxes indicate sources from which thermal optical emissions have been observed in addition to thermal x-rays. Simulations with Fe (H) envelopes are displayed by solid (dashed) curves; those including (excluding) the effects of superfluidity are in red (blue). The upper four curves include cooling from modified Urca processes only; the lower two curves allow cooling with direct Urca processes and neglect the effects of superfluidity. Models forbidding direct Urca processes are relatively independent of M and superfluid properties. The yellow region encompasses cooling curves for models with direct Urca cooling including superfluidity.

alignment. The angular momentum observed to be transferred between these components, in the case of the Vela pulsar, implies that at least 1.4% of the star's moment of inertia resides within the crust (*64*), leading to the *M-R* limit in Fig. 2. However, observations of long-period (~1 year) precesssion in isolated pulsars appear to be inconsistent with the crustal glitch model (*65*).

Quasi-periodic oscillations. Quasi-periodic oscillators (QPOs) are accreting neutron stars that display quasi-periodic behavior in their x-ray emissions. Generally, their power spectra contain a number of features, the most prominent of which are twin high-frequency peaks near 1 kHz, separated by about 300 Hz. An early interpretation of these peaks, offered in the sonic point beat-frequency model (*66*), implies a relatively large neutron star mass, $M \lesssim 2\ M_{\odot}$ (*67*). This model holds that the higher peak frequency is the orbital frequency of the inner edge of the accretion disk and that the separation of the peaks is either once or twice the neutron star's spin rate, but fails to account for the observed variations in peak separation as a function of the lower peak frequency. Therefore, a variety of other models, most but not all based upon rotational phenomenona, are under consideration (*67*). However, none of these models seems to be wholly satisfactory in explaining the observations (*67*).

Future Prospects

Future observations of binary pulsars and isolated neutron stars hold the promise of effective constraints on neutron star maximum masses, radii, and internal compositions. The importance of the nuclear symmetry energy for neutron stars and supernovae has not been overlooked by the nuclear physics community. New accelerator experiments, including high-resolution studies of the neutron skin thickness (which is sensitive to the symmetry energy function S_v) by parity-violating electron scattering on Pb^{208}, are planned (*68*). Anticipated studies of extremely neutron-rich nuclei with rare-isotope accelerators (*31*) will probe conditions intermediate between laboratory nuclei and neutron star matter. Planned intermediate-energy heavy-ion experiments (*69*) could establish the in-medium properties of pions and kaons that are crucial for delimiting the extent of Bose condensation in dense matter. Hypernucleus experiments (*70*) will shed light on strong interaction couplings of strangeness-bearing hyperons likely to occur in dense matter.

A new generation of neutrino observatories also hold great potential for studies of proto–neutron star evolution and neutron star structure. Neutrino observations of supernovae, validated by the serendipitous observations of SN 1987A, which yielded about 20 neutrinos, should detect thousands of neutrinos from a galactic supernova (*71*, *72*). This could yield neutron star binding energies to a few percent accuracy and provide estimates of their masses, radii, and interior compositions, as well as details of neutrino opacities in dense matter. Neutrino fluxes from proto–neutron stars with and without exotica (hyperons, Bose condensates, and quarks) have been investigated in (*13*, *21*).

Gravitational radiation is expected from asymmetric spinning compact objects, from mergers involving neutron stars and black holes, and from gravitational-collapse supernovae (*73*). Depending on the internal viscous forces in rotating neutron stars, gravitational radiation could drive an instability in r-modes of nonradial pulsations to grow on a time scale of tens of seconds (*74*). Mergers (*75*) can be observed to great distances. Detectors due to begin operation over the next decade, including LIGO (Laser Interferometer Gravitational-Wave Observatory), VIRGO (Italian-French Laser Interferometer Collaboration), GEO600 (British-German Cooperation for Gravity Wave Experiment), and TAMA (Japanese Interferometric Gravitational-Wave Project), could see up to hundreds of mergers per year (*76*). Binary mergers can yield important information, including the masses (*73*) and mass-to-radius ratios of the binary's components and possibly details of their inspiraling orbits (*77*).

Table 1. Neutron star mass measurements (1σ uncertainties).

Object	Mass ($M_{\odot}$)	Ref.	Object	Mass ($M_{\odot}$)	Ref.
X-ray binaries					
4U1700-37*	$2.44^{+0.27}_{-0.27}$	(*80*)	Vela X-1†	$1.86^{+0.16}_{-0.16}$	(*81*, *82*)
Cyg X-2	$1.78^{+0.23}_{-0.23}$	(*83*)	4U1538-52	$0.96^{+0.19}_{-0.16}$	(*84*)
SMC X-1	$1.17^{+0.16}_{-0.16}$	(*84*)	LMC X-4	$1.47^{+0.22}_{-0.19}$	(*84*)
Cen X-3	$1.09^{+0.30}_{-0.26}$	(*84*)	Her X-1	$1.47^{+0.12}_{-0.18}$	(*84*)
XTE J2123-058	$1.53^{+0.30}_{-0.42}$	(*85*, *86*)	2A 1822-371	>0.73	(*87*)
Mean = 1.53 $M_{\odot}$, weighted mean = 1.48 $M_{\odot}$					
Neutron star–neutron star binaries					
1518+49	$1.56^{+0.13}_{-0.44}$	(*88*)	1518+49 companion	$1.05^{+0.45}_{-0.11}$	(*88*)
1534+12	$1.3332^{+0.0010}_{-0.0010}$	(*88*)	1534+12 companion	$1.3452^{+0.0010}_{-0.0010}$	(*88*)
1913+16	$1.4408^{+0.0003}_{-0.0003}$	(*88*)	1913+16 companion	$1.3873^{+0.0003}_{-0.0003}$	(*88*)
2127+11C	$1.349^{+0.040}_{-0.040}$	(*88*)	2127+11C companion	$1.363^{+0.040}_{-0.040}$	(*88*)
J0737-3039A	$1.337^{+0.005}_{-0.005}$	(*46*)	J0737-3039B	$1.250^{+0.005}_{-0.005}$	(*46*)
Mean = 1.34 $M_{\odot}$, weighted mean = 1.41 $M_{\odot}$					
Neutron star–white dwarf binaries					
B2303+46	$1.38^{+0.06}_{-0.10}$	(*88*)	J1012+5307	$1.68^{+0.22}_{-0.22}$	(*89*)
J1713+0747‡	$1.54^{+0.07}_{-0.08}$	(*90*)	B1802-07	$1.26^{+0.08}_{-0.17}$	(*88*)
B1855+09‡	$1.57^{+0.12}_{-0.11}$	(*90*)	J0621+1002	$1.70^{+0.32}_{-0.29}$	(*91*)
J0751+1807	$2.20^{+0.20}_{-0.20}$	(*92*, *93*)	J0437-4715	$1.58^{+0.18}_{-0.18}$	(*94*)
J1141-6545	$1.30^{+0.02}_{-0.02}$	(*95*)	J1045-4509	<1.48	(*88*)
J1804-2718	<1.70	(*88*)	J2019+2425	<1.51	(*96*)
Mean = 1.58 $M_{\odot}$, weighted mean = 1.34 $M_{\odot}$					
Neutron star–main sequence binary					
J0045-7319	$1.58^{+0.34}_{-0.34}$	(*88*)			

*Could possibly be a black hole, due to lack of pulsations. †Data from (*81*) used. ‡Reflects binary period–white dwarf mass constraint from (*97*).

References and Notes

1. G. Baym, C. J. Pethick, *Annu. Rev. Nucl. Part. Sci.* **25**, 75 (1975).
2. G. Baym, C. J. Pethick, *Annu. Rev. Astron. Astrophys.* **17**, 415 (1979).
3. H. Heiselberg, V. Pandharipande, *Annu. Rev. Nucl. Part. Sci.* **50**, 481 (2000).
4. N. K. Glendenning, *Astrophys. J.* **293**, 470 (1985).
5. N. K. Glendenning, *Compact Stars, Nuclear Physics, Particle Physics and General Relativity* (New York, Springer, 1997).
6. See *Mesons in Nuclei*, vol. 3, M. Rho, D. Wilkinson, Eds. (North-Holland, Amsterdam, 1979).
7. D. B. Kaplan, A. E. Nelson, *Phys. Lett.* **B175**, 57 (1986).
8. D. B. Kaplan, A. E. Nelson, *Phys. Lett.* **B179** 409 E (1986).
9. J. C. Collins, M. J. Perry, *Phys. Rev. Lett.* **34**, 1353 (1975).
10. C. Alcock, A. Olinto, *Annu. Rev. Nucl. Part. Sci.* **38**, 161 (1988).
11. D. Page, V. V. Usov, *Phys. Rev. Lett.* **89**, 131101 (2002).
12. For a review, see A. Burrows, *Nature* **403**, 727 (2000).
13. A. Burrows, J. M. Lattimer, *Astrophys. J.* **307**, 178 (1986).
14. K. Hirata *et al.*, *Phys. Rev. Lett.* **58**, 1490 (1987).
15. R. M. Bionta *et al.*, *Phys. Rev. Lett.* **58**, 1494 (1987).
16. See, *e.g.* A. Burrows and J.M. Lattimer, *Astrophys. J.* **318**, L63 (1987).
17. C. E. Rhoades, R. Ruffini, *Phys. Rev. Lett.* **32**, 324 (1974).
18. J. M. Weisberg, J. H. Taylor, in *Radio Pulsars*, M. Bailes, D. J. Nice, S. E. Thorsett, Eds. (Astron. Soc. Pac. Conf. Ser. 302, San Francisco, 2003).
19. P. Haensel, J. L. Zdunik, F. Douchin, *Astron. Astrophys.* **385**, 301 (2002).
20. A. Burrows, *Astrophys. J.* **334**, 891 (1988).
21. M. Prakash, J. M. Lattimer, R. F. Sawyer, R. R. Volkas, *Annu. Rev. Nucl. Part. Sci.* **51**, 295 (2001).
22. C. Fransson, C. Kozma, *New Astron. Rev.* **46**, 487 (2002).
23. R. C. Tolman, *Proc. Natl. Acad. Sci. U.S.A.* **20**, 3 (1934).
24. J. R. Oppenheimer, G. M. Volkov, *Phys. Rev.* **55**, 374 (1939).
25. M. S. R. Delgaty, K. Lake, *Comput. Phys. Commun.* **115**, 395 (1998).
26. J. M. Lattimer, M. Prakash, D. Masak, A. Yahil, *Astrophys. J.* **355**, 241 (1990).

27. J. M. Lattimer, M. Prakash, *Astrophys. J.* **550**, 426 (2001).
28. J. L. Friedman, L. Parker, J. R. Ipser, *Astrophys. J.* **304**, 115 (1986).
29. P. Haensel, M. Salgago, S. Bonazzola, *Astron. Astrophys.* **296**, 745 (1995).
30. M. Ashworth, A. G. Lyne, F. G. Smith, *Nature* **301**, 313 (1983).
31. See, e.g., http://citeseer.nj.nec.com/332186.html (2000).
32. C. J. Pethick, D. G. Ravenhall, *Annu. Rev. Nucl. Part. Sci.* **45**, 429 (1995).
33. P. W. Anderson, N. Itoh, *Nature* **256**, 25 (1975).
34. N. K. Glendenning, *Phys. Rev. D* **46**, 1274 (1992).
35. M. Alford, *Annu. Rev. Nucl. Part. Sci.* **51**, 131 (2001).
36. P. F. Bedaque, T. Schafer, *Nucl. Phys.* **A697**, 802 (2002).
37. The term "Urca" was taken from a now defunct, but once glamorous, casino of that name in Rio de Janeiro where gamblers continuously lost money. For a review with historical commentary on direct and modified Urca processes, see (*78*).
38. J. M. Lattimer, C. J. Pethick, M. Prakash, P. Haensel, *Phys. Rev. Lett.* **66**, 2701 (1991).
39. S. Tsuruta, *Phys. Rep.* **292**, 1 (1998).
40. D. G. Yakovlev, A. D. Kaminker, K. P. Levenfish, *Astron. Astrophys.* **343**, 650 (1999).
41. G. Chabrier, A. Y. Potekhin, D. G. Yakovlev, *Astrophys. J.* **477**, L99 (1997).
42. E. Flowers, M. Ruderman, P. Sutherland, *Astrophys. J.* **205**, 541 (1976).
43. D. Page, J. M. Lattimer, M. Prakash, A. W. Steiner, preprint available at http://arxiv.org/abs/astro-ph/0403657.
44. N. Manchester, J. H. Taylor, *Pulsars* (Freeman, San Francisco, 1977).
45. Shapiro delay is the additional time required for light to traverse the curved space near a massive object compared to flat space. See (*79*).
46. A. G. Lyne *et al.*, *Science* **303**, 1153 (2004).
47. H. A. Bethe, G. E. Brown, *Astrophys. J.* **506**, 780 (1998).
48. D. Sanwal, G. G. Pavlov, V. E. Zavlin, M. A. Teter, *Astrophys. J.* **574**, L61 (2002).
49. J. Cottam, F. Paerels, M. Mendez, *Nature* **420**, 51 (2002).
50. C. J. Hailey, K. Mori, *Astrophys. J.* **578**, L133 (2002).
51. R. Romani, *Astrophys. J.* **313**, 718 (1987).
52. G. G. Pavlov, V. E. Zavlin, J. Trümper, R. Neuhäuser, *Astrophys. J.* **472**, L33 (1996).
53. K. Mori, C. J. Hailey, *Astrophys. J.* **564**, 914 (2002).
54. V. Burwitz *et al.*, *Astron. Astrophys.* **379**, L35 (2001).
55. J. J. Drake *et al.*, *Astrophys. J.* **572**, 996 (2002).
56. P. A. Caraveo, G. F. Bignami, R. Mignani, L. G. Taff, *Astrophys. J.* **461**, L91 (1996).
57. D. L. Kaplan, M. H. van Kerkwijk, J. Anderson, *Astrophys. J.* **571**, 477 (2002).
58. F. M. Walter, J. M. Lattimer, *Astrophys. J.* **576**, L145 (2002).
59. W. F. Brisken, S. E. Thorsett, A. Golden, W. M. Goss, *Astrophys. J.* **593**, L898 (2003).
60. E. F. Brown, L. Bildsten, R. E. Rutledge, *Astrophys. J.* **504**, L95 (1998).
61. R. E. Rutledge *et al.*, *Astrophys. J.* **578**, 405 (2002).
62. C. O. Heinke, J. E. Grindlay, D. A. Lloyd, P. D. Edmonds, *Astrophys. J.* **588**, 452 (2003).
63. P. O. Slane, D. J. Helfand, S. S. Murray, *Astrophys. J.* **571**, L45 (2002).
64. B. Link, R. I. Epstein, J. M. Lattimer, *Phys. Rev. Lett.* **83**, 3362 (1999).
65. B. Link, *Phys. Rev. Lett.* **91**, 101101 (2003).
66. D. Psaltis *et al.*, *Astrophys. J.* **501**, L95 (1998).
67. M. van der Klis, *Annu. Rev. Astron. Astrophys.* **38**, 717 (2000).
68. R. Michaels, P.A. Souder, Jefferson Laboratory Proposal PR-00-003 (2000).
69. See, e.g., www-aix.gsi.de.
70. See, e.g., http://jkj.tokai.jaeri.go.jp.
71. A. Burrows, D. Klein, R. Gandhi, *Phys. Rev. D.* **45**, 3361 (1992).
72. C. K. Jung, in *AIP Conf. Proc. No. 533*, M. V. Diwan, C. K. Jung, Eds. (American Institute of Physics, New York, 2000), pp. 29–34.
73. For a readable account, see K. S. Thorne, http://arxiv.org/abs/gr-qc/9704042.
74. For a review, see L. Lindblom, http://arxiv.org/abs/astro-ph/0101136.
75. J. M. Lattimer, D. N. Schramm, *Astrophys. J.* **192**, L145 (1974).
76. V. Kalogera *et al.*, *Astrophys. J.* **601**, L179 (2004); preprint available at http://arxiv.org/abs/astro-ph/0312101.
77. M. Prakash, J. M. Lattimer, *J. Phys. G Nucl. Part. Phys.* **30**, S451 (2003).
78. C. J. Pethick, *Rev. Mod. Phys.* **64**, 1133 (1992).
79. I. I. Shapiro, *Phys. Rev. Lett.* **26**, 789 (1964).
80. J. S. Clark *et al.*, *Astron. Astrophys.* **392**, 909 (2002).
81. H. Quaintrell *et al.*, *Astron. Astrophys.* **401**, 303 (2003).
82. O. Barziv, L. Karper, M. H. van Kerkwijk, J. H. Telging, J. van Paradijs, *Astron. Astrophys.* **377**, 925 (2001).
83. J. A. Orosz, E. Kuulkers, *Mon. Not. R. Astron. Soc.* **305**, 132 (1999).
84. M. H. van Kerkwijk, J. van Paradijs, E. J. Zuiderwijk, *Astron. Astrophys.* **303**, 497 (1995).
85. J. A. Tomsick, W. A. Heindl, D. Chakrabarty, P. Kaaret, *Astrophys. J.* **581**, 570 (2002).
86. J. A. Tomsick, D. M. Gelino, personal communication.
87. P. G. Jonker, M. van der Klis, P. J. Groot, *Mon. Not. R. Astron. Soc.* **339**, 663 (2003).
88. S. E. Thorsett, D. Chakrabarty, *Astrophys. J.* **512**, 288 (1999).
89. Ch. Lange *et al.*, *Mon. Not. R. Astron. Soc.* **326**, 274 (2001).
90. D. J. Nice, E. M. Splaver, I. H. Stairs, in *Radio Pulsars*, M. Bailes, D. J. Nice, S. E. Thorsett, Eds. (Astron. Soc. Pac. Conf. Ser. 302, San Francisco, 2003).
91. E. M. Splaver *et al.*, *Astrophys. J.* **581**, 509 (2002).
92. D. J. Nice, E. M. Splaver, I. H. Stairs, *IAU Symp. 218, ASP Conference Proceedings*, F. Camilo, B. M. Gaensler, Eds.; preprint available at http://arxiv.org/abs/astro-ph/0311296.
93. D. J. Nice, personal communication (2004).
94. W. van Straten *et al.*, *Nature* **412**, 158 (2001).
95. M. Bailes, S. M. Ord, H. S. Knight, A. W. Hotan, *Astrophys. J.* **595**, L49 (2003).
96. D. J. Nice, E. M. Splaver, I. H. Stairs, *Astrophys. J.* **549**, 516 (2001).
97. T. M. Tauris, G. J. Savonije, *Astron. Astrophys.* **350**, 928 (1999).
98. We thank D. Page for providing Fig. 3 and the cooling curves illustrated in Fig. 4. This work was supported in part by the U.S. Department of Energy grant DE-AC02-87ER40317 and by NSF grant INT-9802680.

REVIEW

Observational Properties of Pulsars

R. N. Manchester

Pulsars are remarkable clocklike celestial sources that are believed to be rotating neutron stars formed in supernova explosions. They are valuable tools for investigations into topics such as neutron star interiors, globular cluster dynamics, the structure of the interstellar medium, and gravitational physics. Searches at radio and x-ray wavelengths over the past 5 years have resulted in a large increase in the number of known pulsars and the discovery of new populations of pulsars, posing challenges to theories of binary and stellar evolution. Recent images at radio, optical, and x-ray wavelengths have revealed structures resulting from the interaction of pulsar winds with the surrounding interstellar medium, giving new insights into the physics of pulsars.

Pulsars are naturally occurring celestial objects whose defining characteristic is that the observed emission is a highly periodic pulse train. For known pulsars, the pulse period lies between 1.5 ms and 11 s. These pulsations probably originate as beamed emission from rotating neutron stars—tiny stars, composed predominantly of neutrons, that are formed in the supernova explosions that mark the endpoint of the evolution of massive stars (*1*). The large mass and small radius of a neutron star allows rotation at speeds approaching 1000 revolutions per second and also accounts for the extraordinary stability of the periodicity. Pulsars are also characterized by extremely strong magnetic fields, up to 10^{15} G (10^{11} T) in some cases. The combination of rapid rotation and a strong magnetic field means that a pulsar is an efficient dynamo, generating electric fields of 10^{12} V cm^{-1} or more near its surface. Charged particles are accelerated to ultrarelativistic energies in these large fields, leading to an electron-positron pair production avalanche and ultimately to the generation of a radiation beam. The electrodynamics of the pulsar magnetosphere are complicated [see, e.g., (*2*)], and neither these nor the mechanism responsible for the beamed emission are well understood. Nonetheless, a model in which the radiation is beamed outward from field lines emanating from the magnetic polar caps explains many of the observed properties (*3*).

Although pulsar periods are very stable, they are not constant. All pulsars lose energy, either to magnetic dipole radiation (electromagnetic radiation with a frequency equal to the

Australia Telescope National Facility, Commonwealth Scientific and Industrial Research Organisation (CSIRO), Post Office Box 76, Epping, New South Wales 1710, Australia. E-mail: dick.manchester@csiro.au

The Physics of Neutron Stars

J. M. Lattimer and M. Prakash

Science **304** (5670), 536-542.
DOI: 10.1126/science.1090720